NAVAL POSTGRADUATE SCHOOL
Monterey, California

THESIS

SIMULATION OF PROPOSED
20 KW KLYSTRON FREE ELECTRON LASER

by

R. Eric LeGear

June 1998

Thesis Advisor: William B. Colson
Second Reader: Robert L. Armstead

Approved for public release; distribution is unlimited.

REPORT DOCUMENTATION PAGE

Form Approved
OMB No. 0704-0188

1. AGENCY USE ONLY *(Leave blank)*	2. REPORT DATE	3. REPORT TYPE AND DATES COVERED
	June 1998	Master's Thesis

4. TITLE AND SUBTITLE
Simulation of Proposed 20 KW Klystron Free Electron Laser

5. FUNDING NUMBERS

6. AUTHOR(S)
LeGear, R. Eric

7. PERFORMING ORGANIZATION NAME(S) AND ADDRESS(ES)
Naval Postgraduate School
Monterey, CA 93943-5000

8. PERFORMING ORGANIZATION REPORT NUMBER

9. SPONSORING / MONITORING AGENCY NAME(S) AND ADDRESS(ES)

10. SPONSORING / MONITORING AGENCY REPORT NUMBER

11. SUPPLEMENTARY NOTES
The views expressed in this thesis are those of the author and do not reflect the official policy or position of the Department of Defense or the U.S. Government.

12a. DISTRIBUTION / AVAILABILITY STATEMENT
Approved for public release; distribution is unlimited.

12b. DISTRIBUTION CODE

13. ABSTRACT

The Free Electron Laser (FEL) is a potential solution for the U.S. Navy's anti-ship missile point defense by providing an evolutionary increase in weapon accuracy. To become an effective weapon, the FEL will need to provide an average optical power of approximately one MW. Towards this goal, the Thomas Jefferson National Accelerator Facility (TJNAF) in Newport News, Virginia is constructing the first kW FEL, and desires to improve the design to 20 kW while maintaining less than 6% energy spread. Using a klystron undulator is one potential way to accomplish this. Given design parameters of a proposed free electron laser by TJNAF, this study quantifies via simulation the behaviors of gain, power and energy spread as functions of desynchronism and a klystron's dispersive strength. Specifically, it shows that a conventional undulator appears capable of meeting all TJNAF design requirements.

14. SUBJECT TERMS	15. NUMBER OF PAGES
Free Electron Laser, Undulator, Klystron	56
	16. PRICE CODE

17. SECURITY CLASSIFICATION OF REPORT	18. SECURITY CLASSIFICATION OF THIS PAGE	19. SECURITY CLASSIFICATION OF ABSTRACT	20. LIMITATION OF ABSTRACT
Unclassified	Unclassified	Unclassified	UL

NSN 7540-01-280-5500

Standard Form 298 (Rev. 2-89)
Prescribed by ANSI Std. 239-18

Approved for public release; distribution is unlimited

SIMULATION OF PROPOSED 20 KW KLYSTRON FREE ELECTRON LASER

R. Eric LeGear
Lieutenant, United States Navy
B.S., University of South Carolina, 1990

Submitted in partial fulfillment of the
requirements for the degree of

MASTER OF SCIENCE IN APPLIED PHYSICS

from the

NAVAL POSTGRADUATE SCHOOL
June 1998

ABSTRACT

The Free Electron Laser (FEL) is a potential solution for the U.S. Navy's anti-ship missile point defense by providing an evolutionary increase in weapon accuracy. To become an effective weapon, the FEL will need to provide an average optical power of approximately one MW. Towards this goal, the Thomas Jefferson National Accelerator Facility (TJNAF) in Newport News, Virginia is constructing the first kW FEL, and desires to improve the design to 20 kW while maintaining less than 6% energy spread. Using a klystron undulator is one potential way to accomplish this. Given design parameters of a proposed free electron laser by TJNAF, this study quantifies via simulation the behaviors of gain, power and energy spread as functions of desynchronism and a klystron's dispersive strength. Specifically, it shows that a conventional undulator appears capable of meeting all TJNAF design requirements.

TABLE OF CONTENTS

I. INTRODUCTION

A. THE DEFICIENCY IN CURRENT ANTI-SHIP MISSILE POINT DEFENSE

1. Current Point Defense System Description

Since 1978, the Phalanx Close-In Weapon System (CIWS) has been the U.S. Navy's last line of defense against anti-ship cruise missiles. CIWS is currently installed aboard all combatants, amphibious landing and logistics support ships. CIWS uses a 20-mm Gattling gun with a microwave radar that tracks both the incoming missile as well as the outgoing CIWS rounds. This allows the mount to autonomously adjust the stream of rounds onto the target. Engagements can begin out to 2 km with a minimum engagement range of 100 m.

2. Performance Appraisal Using Simulation

Just how effective is this system? CIWS has never been challenged in combat. We must therefore resort to simulation to predict its performance against real world threats. Modeling the path of CIWS rounds is a simple problem in classical physics. For the purpose of this analysis, the effects of gravity and air drag are included, and perfect tracking by CIWS' radar is assumed.

Every gun system suffers from an effect called dispersion. It is the error incurred when rounds do not go precisely where they are directed. The reasons for this effect are numerous: barrel vibrations, variations in shell manufacturing, etc. Despite reduction efforts in this area, CIWS still experiences a dispersion of 3 millirads or 0.17 degrees [1]. It may not sound like much, but it has a large affect upon performance.

A typical CIWS burst is approximately 200 rounds. Given a stationary missile with a 20 cm radius (typical of today's cruise missile inventory) at 750 m range (less than half the maximum engagement range), only 3 rounds out of 200 actually hit [1]! Figure 1 graphically shows these results.

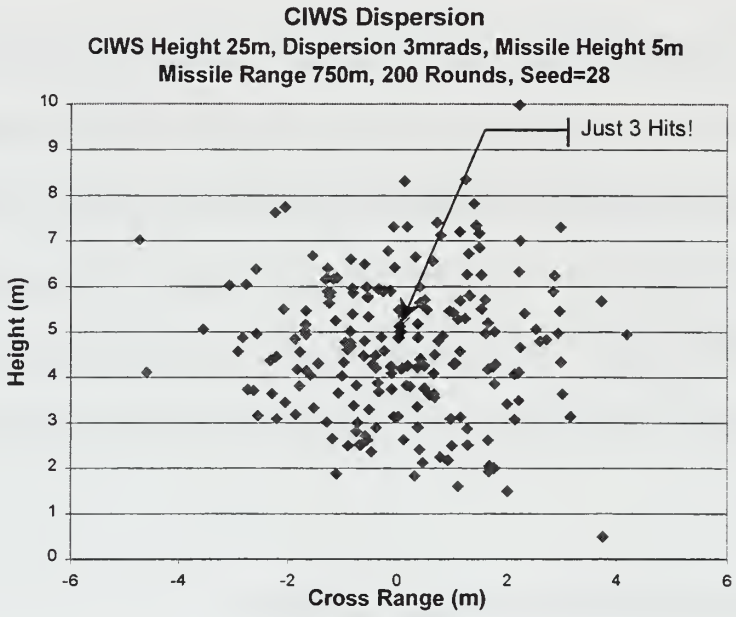

Figure 1. CIWS Dispersion

This makes the intercept probability of any one round at 750 m just 1.5%. Figure 2 shows the intercept probability behavior as a function of decreasing range [1]. The maximum probability is just over 35% at 100 m (CIWS' minimum engagement range). Beyond 700 m, the probability of hit drops off to almost nothing.

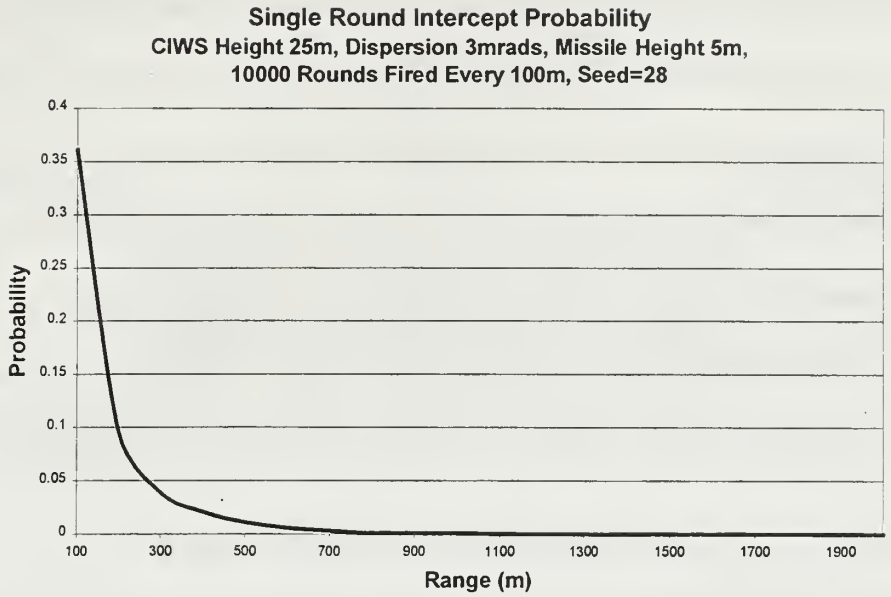

Figure 2. Single Round Intercept Probability

The previous analysis has focused on hitting the missile once. Unfortunately, missiles rarely die from the first hit. Rather, it takes an average of six to ten hits to either destroy the missile's aerodynamics or ignite its warhead [1]. To continue with our analysis, let us assume eight hits, and that the missile is moving at 300 m/s (slow by today's standard) on a constant trajectory inbound to the ship. At what range is this missile typically destroyed?

The CIWS firing rate is 50 rounds/s, and each round has an initial velocity of 1,200 m/s. This means that an incoming missile encounters approximately 21 rounds with every 100 m section in decreasing range to the ship. The number of CIWS hits on the missile at a particular range is equal to 21 rounds multiplied by the single round intercept probabilities shown in Figure 2. The accumulated hit count as the missile approaches the ship reaches eight at approximately 150 m. If we simulate debris

trajectories from a typical warhead at a height 5 m above the water and 150 m range, more than half of the debris strikes the ship [1]!

So for even a quite simple threat, the ship will suffer damage. In today's warfare of zero tolerable losses, any amount of ship damage could force its withdrawal from the theater of operations. Given today's sophisticated, anti-ship cruise missile environment, CIWS can not be counted upon to capably defend our fleet. Therefore, we should pursue research on a point air defense system that is much more accurate with longer range.

B. POTENTIAL ANSWER: THE FREE ELECTRON LASER

1. Basic Description

A potential long-term answer to the U.S. Navy's point air defense problem is a high-energy laser. One candidate is the Free Electron Laser (FEL). In its simplest description, a FEL is made of two major components: an electron accelerator and an undulator. The accelerator propels electrons to near the speed of light. The relativistic electrons then enter the undulator, which consists of a series of alternating magnets. If we assume a planar undulator (2D only), these alternating magnets produce a sinusoidal magnetic field along the undulator axis. As the electrons pass by each magnet, they are deflected slightly from side to side. This periodic action converts the straight electron beam path into an oscillating one. As the electrons oscillate in the presence of light, they bunch together and emit coherent light radiation.

There are two types of free electron lasers: oscillators and amplifiers. In an oscillator (Figure 3), the optical field (seen in gray) is stored between two mirrors with the undulator in the middle. With each pass of the optical wave through the undulator, it

receives more and more energy from the electron beam. Between one and ten percent is extracted from the optical cavity to make a weapon.

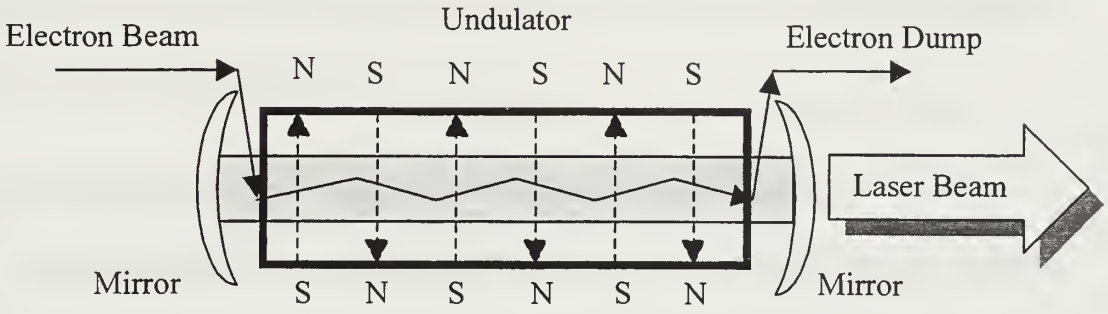

Figure 3. Oscillating FEL

An amplifier is similar, but lacks the mirrors at either end of the undulator. Here, the optical wave makes only a single pass down the undulator. This design works well if the optical field already exists, the FEL gain is large, and the output power is enough to destroy any mirrors.

2. Potential Advantages Over The Current Point Defense System

While FEL offers several advantages over CIWS, the primary ones are increased range and improved accuracy. Although CIWS has a maximum engagement range of 2 km, the previous analysis shows that consummation of even a simple engagement may not occur until a few hundred meters. In addition to subjecting the ship to missile debris at this short kill range, CIWS is unlikely to have sufficient time to engage a second trailing missile. On the other hand, the FEL's effective range is from 5 to 10 km. This is a tremendous tactical advantage since it prevents ship damage from debris and greatly improves our ability to engage a second and even third successive threat.

A second advantage is improved accuracy. Laser weapons do not suffer from dispersion. Through the use of optics, we can focus a laser's energy within the cross-sectional area of a missile even at 5 to 10 km.

3. Potential Advantages Over Chemical Lasers

The U.S. Army and Air Force are developing high-energy chemical lasers for battlefield air defense and Theater Ballistic Missile Defense (TBMD) respectfully. Why not choose such a laser for maritime defense? There are two main disadvantages. First, the chemical process chosen for each laser application dictates its wavelength. This makes the weapon inflexible to changes during and after the design process. A second disadvantage is that high power chemical lasers produce large quantities of hazardous waste that can not be disposed of at sea. This greatly complicates tailoring such a laser for maritime employment. For these reasons, chemical lasers may not be the Navy's answer.

A free electron laser does not produce hazardous waste, and its wavelength is tunable by three means: changing the undulator's wavelength (distance between magnets), the undulator's magnetic field amplitude or the accelerator's electron beam energy. This provides great flexibility in optimizing a laser within its operating environment.

4. Power Required to Destroy a Missile

Just how much optical power is required to destroy a missile? For ship self-defense, the goal is to cause structural failure of the missile's nose cone rather than ignite its warhead. Let us assume that the nose of the missile is approximately 1 L in volume

consisting of about $3x10^{25}$ atoms. In a typical solid, we need approximately 1 eV (electron volt) of energy to remove each atom. This translates to 5 MJ of total energy. If we permit 2 to 3 seconds per engagement, this means we need 1.5 to 2 MW of average power delivered at the missile [1].

5. Present Stage of Research & Development

How close are we to achieving a MW FEL suitable for shipboard deployment? In the 1980's, the Strategic Defense Initiative (SDI) goal was to design a 10 MW FEL with no intermediate steps at smaller powers. Scientists completed the design, and if built it would have been quite large and costly. With a change in national priorities, the U.S. Government cancelled SDI before completion of the FEL project. Since then, several laboratories have worked with operational FELs in the 10 watt range. Currently, the Thomas Jefferson National Accelerator Facility (TJNAF) in Newport News, Virginia has undertaken the next step by constructing a kW FEL. Operation begins in the summer of 1998.

C. PURPOSE OF THIS THESIS

Once TJNAF has successfully proven the kW FEL, their next design step is to increase output to 20kW. There are several design initiatives worth exploring to achieve this. One is to use a special type of undulator called a klystron. The purpose of this thesis is to quantify the steady state gain and final power behaviors of a proposed 20 kW klystron.

II. FEL THEORY

A. ELECTRON BEHAVIOR WITHIN THE UNDULATOR

To understand how a FEL works, it is first important to comprehend the electron behavior within the undulator [2]. They travel at relativistic velocities, and their motion is described using the principles of classical physics. For the undulator, let us use the coordinate system shown in Figure 4:

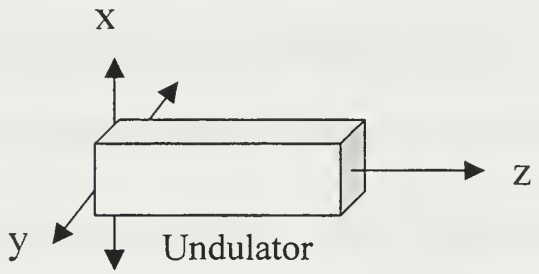

Figure 4. Undulator Coordinate System

The undulator's circularly polarized magnetic field can be described by the equation:

$$\bar{B}_O = B[\cos k_O z, \sin k_O z, 0] \tag{1}$$

where B is the magnetic field amplitude. $k_O = 2\pi / \lambda_O$ is the undulator wave number,. λ_O is the undulator wavelength (distance between magnets), and z is the distance down the undulator. The generated optical field within the undulator is a circularly polarized plane-wave composed of its own electric and magnetic fields. These optically induced fields can be described by the equations:

$$\vec{E} = E[\cos\Psi, -\sin\Psi, 0] \quad \text{and} \quad \vec{B} = E[\sin\Psi, \cos\Psi, 0] \tag{2}$$

E is the electric and magnetic field magnitudes while $\Psi = kz - \omega t + \phi$. $k = \omega / c$ is the optical field wave number. ω is the optical wave's angular frequency, and ϕ is the optical wave's phase. The speed of light in a vacuum is c, and t is the time.

The Lorentz force equation governs electron motion in the presence of electric and magnetic fields,

$$\frac{d\vec{p}}{dt} = -e\left(\vec{E} + \vec{\beta} \times \vec{B}_T\right) \quad \text{and} \quad \frac{d(\gamma mc^2)}{dt} = -e\left(\vec{v} \cdot \vec{E}\right), \tag{3}$$

where $\vec{p} = \gamma m\vec{v}$ is the electron momentum, m is the electron mass, e is the electron charge, $\vec{v}$ is the electron velocity, $\vec{\beta} = \vec{v} / c$ is the dimensionless electron velocity and $\gamma = \left(1 - \beta^2\right)^{-1/2}$ is the Lorentz factor. From Einstein's relativistic theory, the electron energy is γmc^2. Finally, $\vec{B}_T = \vec{B}_O + \vec{B}$ is the total magnetic field within the undulator. Substituting the definition for momentum into the Lorentz force equation, we can get (3) into the form:

$$\frac{d\gamma\vec{\beta}}{dt} = -\frac{e}{mc}\left(\vec{E} + \vec{\beta} \times \vec{B}_T\right) \quad \text{and} \quad \frac{d\gamma}{dt} = -\frac{e}{mc}\left(\vec{\beta} \cdot \vec{E}\right). \tag{4}$$

We now insert the electric and magnetic fields of (1) and (2) into (4), and simplify the results by splitting $\vec{\beta}$ into two components: $\vec{\beta}_\perp = [\beta_X, \beta_Y, 0]$ and $\vec{\beta}_Z = [0, 0, \beta_Z]$, to arrive at three components:

$$\frac{d(\gamma\vec{\beta}_\perp)}{dt} = -\frac{e}{mc}\left(E(1 - \beta_Z)[\cos\Psi, -\sin\Psi, 0] + B\beta_Z[-\sin k_O z, \cos k_O z, 0]\right), \tag{5}$$

$$\frac{d(\gamma\bar{\beta}_Z)}{dt} = -\frac{e}{mc}\left[0,0,E(\beta_X \cos\Psi - \beta_Y \sin\Psi) + B(\beta_X \sin k_O z - \beta_Y \cos k_O z\right], \qquad (6)$$

$$\text{and} \quad \frac{d\gamma}{dt} = -\frac{e}{mc}E\left(\beta_X \cos\Psi - \beta_Y \sin\Psi\right). \qquad (7)$$

To understand electron behavior within the undulator, we need only use equations (5) and (7) because (6) can be derived from (5) and (7). Concerning equation (5), we can make several simplifying approximations. First, $\beta_Z \approx 1$ so $E(1-\beta_Z) << B\beta_Z$ when $E \approx B$. This allows us to ignore the first term in (5) so that

$$\frac{d\left(\gamma\bar{\beta}_\perp\right)}{dt} = -\frac{eB\beta_Z}{mc}\left[-\sin(k_O z, \cos(k_O z), 0\right]. \qquad (8)$$

After integrating (8), the component equations become:

$$\beta_X = -\frac{eB}{k_O \gamma mc^2}\cos(k_O z) \quad \text{and} \quad \beta_Y = -\frac{eB}{k_O \gamma mc^2}\sin(k_O z). \qquad (9)$$

To further simplify (9), the dimensionless undulator parameter is $K = eB/k_O mc^2$ so:

$$\beta_X = -(K/\gamma)\cos(k_O z) \quad \text{and} \quad \beta_Y = -(K/\gamma)\sin(k_O z) \qquad (10)$$

The next step is to now insert (10) into (7) using the trigonometric identity:

$\cos A \cos B - \sin A \sin B = \cos(A+B)$,

$$\frac{d\gamma}{dt} = \frac{eEK}{\gamma mc}\cos\left(k_O z + \Psi\right), \qquad (11)$$

where $k_O z + \Psi = k_O z + kz - \omega t + \phi = (k_O + k)z - \omega t + \phi$. Define $\zeta = (k_U + k_O)z - \omega t$ as the electron phase in the combined undulater magnetic field and the associated optical fields so that (11) becomes:

$$\frac{d\gamma}{dt} = \dot{\gamma} = \frac{eKE}{\gamma mc}\cos(\zeta + \phi). \qquad (12)$$

Equation (12) looks similar to a simple pendulum equation, but to get it into the right form, we need to express $\dot{\gamma}$ in terms of $\ddot{\zeta}$. Recall the definition for the Lorentz factor: $1/\gamma^2 = 1-\beta^2 = 1-\beta_\perp^2-\beta_z^2$. From (9), $\beta_\perp^2 = K^2/\gamma^2$ so that:

$$\beta_z \approx 1-\frac{1+K^2}{2\gamma^2} \quad \text{and} \quad \dot{\beta}_z = \frac{1+K^2}{\gamma^2}\left(\frac{\dot{\gamma}}{\gamma}\right). \tag{13}$$

Since $\zeta = (k_U + k_O)z - \omega t$,

$$\ddot{\zeta} = (k_O + k)c\dot{\beta}_z . \tag{14}$$

When (14) is substituted into (13), the result is:

$$\frac{\dot{\gamma}}{\gamma} = \frac{\ddot{\zeta}\gamma}{(k_O+k)c}\left(\frac{\gamma^2}{1+K^2}\right). \tag{15}$$

To simplify any further, we need to shift our focus to the interaction of electrons and photons. Photons overtake the electrons as they both proceed down the undulator. When one wavelength of light λ overtakes an electron just as the electron traverses one undulator wavelength λ_O, the FEL is at resonance. Finding how the undulator and optical field wavelengths are related at resonance will enable us to simplify (15), which will in turn allow us to write (12) in the desired simple pendulum form. The time required for an electron to traverse one undulator period is $t_E = \lambda_O / v_z = \lambda_O / \beta_z c$. In the same time, the traveled distance of a photon is $\lambda = ct_E - v_z t_E = ct_E(1-\beta_z)$. Substituting the first condition into the second yields the relationship:

$$\lambda = \frac{\lambda_O(1-\beta_z)}{\beta_z}. \tag{16}$$

Inserting (13) into (16) and rearranging,

$$\frac{\lambda_O}{2\lambda} = \frac{\gamma^2}{1+K^2}. \tag{17}$$

Reverting back now to (15), we can simplify it by substituting in equation (17),

$$\dot{\gamma} = \frac{\ddot{\zeta}\gamma}{(k_O + k)c}\left(\frac{\lambda_O}{2\lambda}\right) = \frac{\ddot{\zeta}\gamma}{(k_O + k)c}\left(\frac{k}{2k_O}\right). \tag{18}$$

The undulator wavelength (cm) is much greater than the laser's optical wavelength (μm) so $k >> k_O$. This allows (18) to simplify to:

$$\dot{\gamma} \approx \frac{\ddot{\zeta}\gamma}{2k_O c}. \tag{19}$$

Finally, inserting (19) into (12), the pendulum equation of electron motion within the undulator is:

$$\ddot{\zeta} = \frac{2k_O eKE}{\gamma^2 m}\cos(\zeta + \phi). \tag{20}$$

It's helpful when designing a FEL to use dimensionless parameters when possible. Such is the case when dealing with time. For an average electron, the time it spends in the undulator is $t = L / v_z = L / \beta_z c \approx L / c$ where L is the undulator length and $\beta_z \approx 1$. The dimensionless time is defined as $\tau = ct / L$ so that τ=0 at the undulator beginning and τ=1 at the end. Rewriting (20) in terms of the second derivative with respect to dimensionless time yields:

$$\ddot{\zeta} = |a|\cos(\zeta + \phi), \tag{21}$$

where the dimensionless optical field is $|a| = 4\pi NeKLE / \gamma^2 mc^2$, the number of undulator periods is $N = L / \lambda_O$, and the open dot represents the derivative with respect to τ.

B. OPTICAL WAVE BEHAVIOR WITHIN THE UNDULATOR

The previous section has detailed electron behavior within the undulator. Now, attention is turned to how the optical wave develops within the undulator [3]. As stated earlier, the optical field is a circularly polarized plane-wave. The wave's vector potential is:

$$\vec{A} = \frac{E(z,t)}{k}[\sin\Psi, \cos\Psi, 0]. \tag{22}$$

$E(z,t)$ is the optical wave's electric field magnitude and $\Psi = kz - \omega t + \phi$. $k = \omega / c$ is the optical wave number, ω is the optical wave's angular frequency and ϕ is the optical phase.

Optical fields obey Maxwell's wave equation:

$$\left(\vec{\nabla}^2 - \frac{1}{c^2}\frac{\partial^2}{\partial t^2}\right)\vec{A} = -\frac{4\pi}{c}\vec{J}_\perp \tag{23}$$

where $\vec{J}_\perp$ is the total transverse beam current. If the expression for $\vec{A}$, (22), is inserted into (23) and the left-hand side of the equation is written out, a quite long and complicated expression results. The left-hand side can be simplified greatly by making the assumptions that the optical wave varies slowly in space with respect to an optical wavelength λ, and varies slowly in time with respect to a single optical period $= \lambda / c$. Mathematically, this means:

$$\frac{dE}{dt} << \omega E, \frac{d\phi}{dt} << \omega\phi \quad \text{and} \quad \frac{dE}{dz} << k_O E, \frac{d\phi}{dz} << k_O\phi. \tag{24}$$

Using (24) to simplify, (23) reduces to:

$$\left(\vec{\nabla}^2 - \frac{1}{c^2}\frac{\partial^2}{\partial t^2}\right)\vec{A} \approx \frac{2}{c}\left(\frac{\partial E}{\partial t}\right)\hat{\varepsilon}_1 - \frac{2E}{c}\left(\frac{\partial \phi}{\partial t}\right)\hat{\varepsilon}_2 = -\frac{4\pi}{c}\vec{J}_\perp \tag{25}$$

where we have defined the two orthogonal unit vectors as:

$$\hat{\varepsilon}_1 = [\cos\Psi, -\sin\Psi, 0] \quad \text{and} \quad \hat{\varepsilon}_2 = [\sin\Psi, \cos\Psi, 0]. \tag{26}$$

Through the slowly-varying amplitude and phase approximation, (25) is converted from a second-order differential equation to two first-order equations:

$$\hat{\varepsilon}_1 \cdot \left(\vec{\nabla}^2 - \frac{1}{c^2}\frac{\partial^2}{\partial t^2}\right)\vec{A} \approx \frac{2}{c}\left(\frac{\partial E}{\partial t}\right) = -\frac{4\pi}{c}\vec{J}_\perp \cdot \hat{\varepsilon}_1 \quad \text{and} \tag{27}$$

$$\hat{\varepsilon}_2 \cdot \left(\vec{\nabla}^2 - \frac{1}{c^2}\frac{\partial^2}{\partial t^2}\right)\vec{A} \approx \frac{2E}{c}\frac{\partial \phi}{\partial t} = -\frac{4\pi}{c}\vec{J}_\perp \cdot \hat{\varepsilon}_2 . \tag{28}$$

Now attention is turned to the right-hand side of Maxwell's equation. The current of a single electron is $\vec{J}_i = -ec\vec{\beta}_\perp \delta^3(\vec{x} - \vec{r}_i)$ where e is the electron charge magnitude, $\vec{\beta}_\perp$ is the dimensionless transverse electron velocity (8), $\delta^3(\vec{x} - \vec{r}_i)$ is the three dimensional Dirac function, and $\vec{r}_i$ is the position of the i'th electron [4]. Expanded out, the transverse current for one electron becomes:

$$\vec{J}_{\perp i} = \frac{e^2 B}{\gamma m \omega}[\cos(k_O z), \sin(k_O z), 0]\delta^3(\vec{x} - \vec{r}_i), \tag{29}$$

where B is the magnitude of the undulator's magnetic field, γ is the Lorentz factor (3), m is the electron mass, and k_O is the undulator's wave number (1). Substituting (29) into (27) and (28), the wave equation becomes:

$$\vec{J}_{\perp i} \cdot \hat{\varepsilon}_1 = \frac{e^2 B}{\gamma m \omega}\cos(\Psi + k_O z)\delta^3(\vec{x} - \vec{r}_i) \tag{30}$$

$$\vec{J}_{\perp i} \cdot \hat{\varepsilon}_2 = \frac{e^2 B}{\gamma m \omega}\sin(\Psi + k_O z)\delta^3(\vec{x} - \vec{r}_i) \tag{31}$$

Equations (30) and (31) deal only with a single electron. The total transverse current is the sum over all electrons. This is represented by averaging $\langle ... \rangle$ over a fixed volume weighted by the electron density ρ resulting in:

$$\frac{1}{c}\left(\frac{\partial E}{\partial t}\right) = -\frac{2\pi e K}{\gamma}\rho\left\langle \cos(\zeta + \phi)\right\rangle \quad \text{and} \tag{32}$$

$$E\left(\frac{1}{c}\frac{\partial \phi}{\partial t}\right) = -\frac{2\pi e K}{\gamma}\rho\left\langle \sin(\zeta + \phi)\right\rangle, \tag{33}$$

where K is the undulator parameter (10) and ζ is the electron phase. Equations (32) and (33) can be simplified by defining the dimensionless current:

$$j = \frac{8N\rho(e\pi KL)^2}{\gamma^3 mc^2}, \tag{34}$$

where L is the undulator length and N is the number of undulator periods (21), and the dimensionless optical field strength $|a|$ in (21). The results are:

$$\dot{|a|} = -j\left\langle \cos(\zeta + \phi)\right\rangle \quad \text{and} \tag{35}$$

$$\dot{\phi} = \frac{j}{|a|}\left\langle \sin(\zeta + \phi)\right\rangle, \tag{36}$$

where $a = |a|e^{i\phi}$. Equations (35) and (36) can be combined back into one equation in complex form:

$$\dot{a} = -j\left\langle e^{-i\zeta}\right\rangle \tag{37}$$

C. LOW GAIN DERIVATION

Gain is the fractional change in power of the optical wave as it makes a single pass down the undulator. As mentioned in the introduction, there are two basic FEL designs: oscillators and amplifiers. Oscillators typically use low current ($j \leq 1$) to build the optical field through multiple passes of the light wave through the undulator and between the mirrors of an optical resonator. Amplifiers on the other hand typically rely upon high current ($j >> 1$) to provide high gain in a single pass. The FEL under construction at Thomas Jefferson National Accelerator Facility is an oscillator design so only low gain is discussed here [5]. See reference [6] for an explanation of high gain behavior.

Using conservation of energy, any change in the optical wave energy is a result of an opposite change in the electron beam energy so that the gain can be calculated by dividing the change in electron beam energy by the optical wave energy. To find this overall change in electron beam energy (which consists of electrons: some gaining and some losing energy (21)), we must first find an expression for the energy change of a single electron, $\Delta\gamma mc^2$.

To help understand single electron behavior, we define the dimensionless electron phase velocity υ as the dimensionless time τ derivative of the electron phase ζ; thus $\dot{\zeta} = \upsilon = L\left[(k_O + k_U)\beta_Z - k_O\right]$. An electron's change in energy is related to its change in phase velocity $\Delta\upsilon$. Since $k >> k_O$, $\Delta\upsilon = Lk\Delta\beta_Z$. Using (13) and (17), the relationship between $\Delta\gamma$ and $\Delta\upsilon$ is:

$$\Delta\upsilon = Lk\Delta\beta_z = N\lambda_O k\Delta\beta_z = 2\pi N\left(\frac{\lambda_O}{\lambda}\right)\Delta\beta_z \approx 2\pi N\left(\frac{2\gamma^2}{1+K^2}\right)\Delta\beta_z \approx 4\pi N\frac{\Delta\gamma}{\gamma}. \quad (38)$$

The energy change of a single electron is then:

$$\Delta\gamma mc^2 = \frac{\gamma mc^2\Delta\upsilon}{4\pi N}. \quad (39)$$

In the case where the optical field is weak ($a << \pi$) and the gain is low ($j << \pi$), there is little change in υ over the entire undulator length. Therefore, using perturbation theory, a solution to the pendulum equation (21) expanded in powers of the initial optical field strength a_O:

$$\zeta(\tau) = \zeta_O + \upsilon_O\tau - \frac{a_O}{\upsilon_O^2}\left[\cos(\zeta_O + \upsilon_O\tau) - \cos\zeta_O + \nu_O\tau\sin\zeta_O\right] + \cdots, \quad (40)$$

and the electron phase velocity becomes:

$$\begin{aligned}\upsilon(\tau,\zeta_O) &= \upsilon_O + \frac{a_O}{\upsilon_O}\left[\sin(\zeta_O + \upsilon_O\tau) - \sin\zeta_O\right] + \\ &\frac{a_O^2}{\upsilon_O^3}\left[-\frac{1}{4}\left(\cos(2\zeta_O + 2\upsilon_O\tau) - \cos 2\zeta_O\right) + \cos\upsilon_O\tau - 1 - \upsilon_O\tau\sin\zeta_O\cos(\zeta_O + \upsilon_O\tau)\right] + \cdots,\end{aligned} \quad (41)$$

where ζ_O and υ_O represent initial values of their respective variables.

The average phase velocity of all sampled electrons within the beam $\langle\upsilon\rangle$ gives the change from the initial phase velocity, $\Delta\upsilon = \langle\upsilon\rangle - \upsilon_O$. This makes the average change in beam energy:

$$\overline{\Delta\gamma mc^2} = \frac{\gamma mc^2\left(\langle\upsilon\rangle - \upsilon_O\right)}{4\pi N}. \quad (42)$$

Equation (41) can be converted by averaging over the initial phases ζ_O:

$$\langle \upsilon \rangle = \frac{1}{2\pi} \int_0^{2\pi} \upsilon(\tau, \zeta_O) d\zeta_O = \frac{a_O^2}{\upsilon_O^3} \left[\cos \upsilon_O \tau - 1 + \frac{1}{2} \upsilon_O \tau \sin \upsilon_O \tau \right]. \tag{43}$$

We must also include the fact that the electron beam radius does not equal the optical beam waist. Conservation of energy only applies within the area where both beams overlap. Therefore, we must introduce a filling factor:

$$F = \frac{r_b^2}{w_O^2}, \tag{44}$$

where r_b is the electron beam radius and w_O is the radius of the optical beam waist. For the whole beam, the number of electrons is the electron density ρ multiplied by the volume dV occupied by the optical beam one wavelength long so that (42) becomes:

$$\overline{\Delta\gamma} mc^2 = \frac{\rho F dV \gamma mc^2 \left(\langle \upsilon \rangle - \upsilon_O \right)}{4\pi N}. \tag{45}$$

The optical energy within the volume dV is $E^2 dV / 4\pi$ so the low gain equation is:

$$G = \frac{\overline{\Delta\gamma} mc^2}{Energy_{OPTICAL}} = \left(\frac{\rho F dV \gamma mc^2 \left(\langle \upsilon \rangle - \upsilon_O \right)}{4\pi N} \right) \left(\frac{4\pi}{E^2 dV} \right) \tag{46}$$

Inserting (34) and (43) into (46), the gain finally becomes:

$$G = \frac{j \left[2 - 2\cos \upsilon_O \tau - \upsilon_O \tau \sin \upsilon_O \tau \right]}{\upsilon_O^3} \tag{47}$$

where F has been absorbed into j for brevity. To gain a better understanding of equation (47), Figure 5 is a plot of final ($\tau = 1$) gain versus the initial electron phase υ_O with j=1.

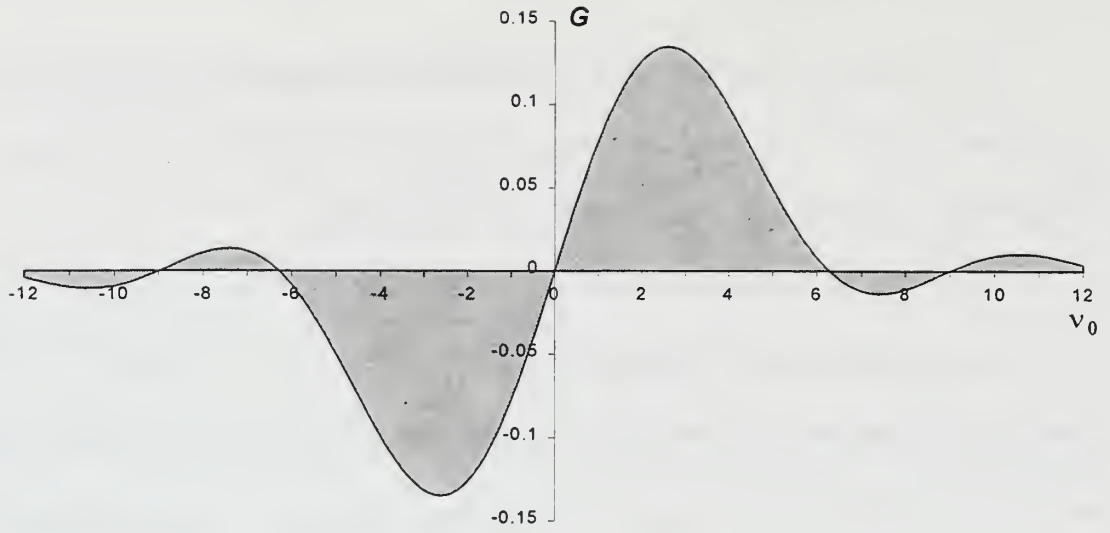

Figure 5. Low Gain Spectrum for Low Current and Weak Fields

Notice that the gain spectrum is anti-symmetric about resonance $\upsilon_O = 0$. Why does resonance result in zero gain? Electrons enter the undulator with a random initial phase ζ_O from -π/2 to 3π/2. When an electron's phase is $\pi/2 < (\zeta+\phi) < 3\pi/2$, equation (21) says the phase acceleration is negative. Negative phase acceleration makes the change in phase velocity $\Delta\upsilon$ also negative. Equation (39) states that when an electron has $-\Delta\upsilon$, it losses energy. That energy is transferred to the optical field thereby increasing the laser's gain. On the to other hand, when an electron's phase is $-\pi/2 < (\zeta+\phi) < \pi/2$, then the phase acceleration is positive so the electron is gaining energy. The only way for the electron to increase in energy is by absorbing energy from optical wave thereby decreasing the laser's gain. If the electrons' initial velocity is at resonance, they

bunch together at $\zeta \approx \pi / 2$ and equal number of electrons gain and lose energy. The net effect is zero optical gain. Figure 6 graphically shows the resonance condition.

Plotted in the main window is the phase space path (ζ versus υ) of 30 electrons as they travel down the undulator (their paths darken as they approach $\tau = 1$). Those electrons that are decreasing in υ are losing energy (increasing the laser's optical energy) and those that are increasing in υ are gaining energy (depleting the laser's optical energy). The numbers of electrons gaining and losing are approximately equal, and they are all approaching the same phase of $\pi / 2$. The top right window depicts gain growth as a function of τ, and it never rises above zero. The lower right graph shows the evolution of the optical phase $\phi(\tau)$.

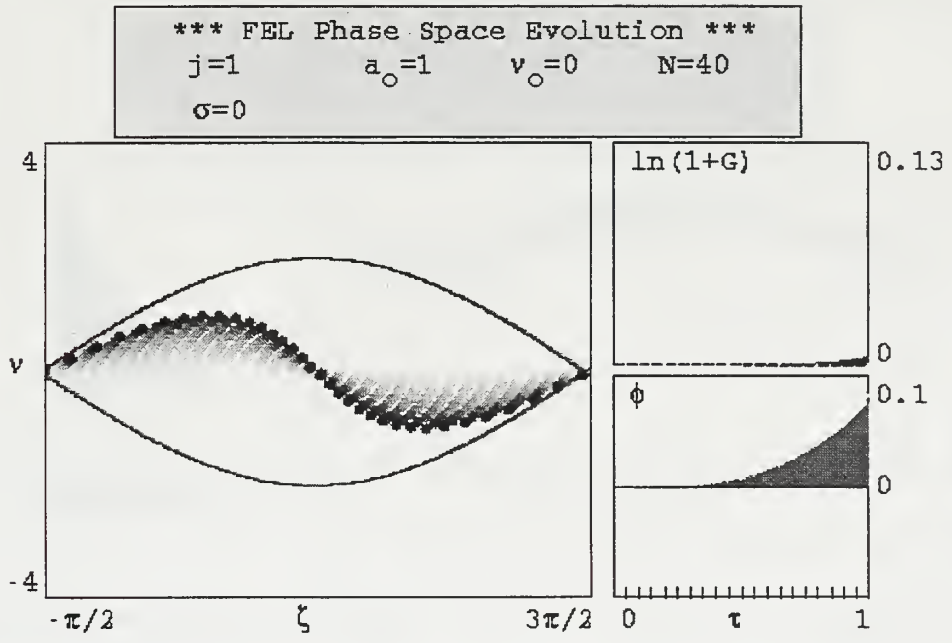

Figure 6. Phase Space Diagram of the Resonance Condition

While the resonance condition is a good case in understanding electron behavior and bunching, it is pointless designing a laser with zero gain. On the other hand, (47) has a maximum positive gain at $\upsilon_o = 2.6$. To help understand why, Figure 7 illustrates this case. Here, more electrons lose phase velocity than gain, and instead of bunching at $\pi/2$, they bunch at π. This can be seen analytically by combining (20) and (39) to yield the fractional change in electron energy:

$$\frac{\dot{\gamma}}{\gamma} = \frac{a_o}{4\pi N}\cos\zeta_o . \tag{48}$$

Equation (48) has the most negative value when $\zeta_o = \pi$. Consequently with $j = 1$ in Figure 7, $\ln(1+G)$ peaks to a maximum value of 0.13, representing 13% gain.

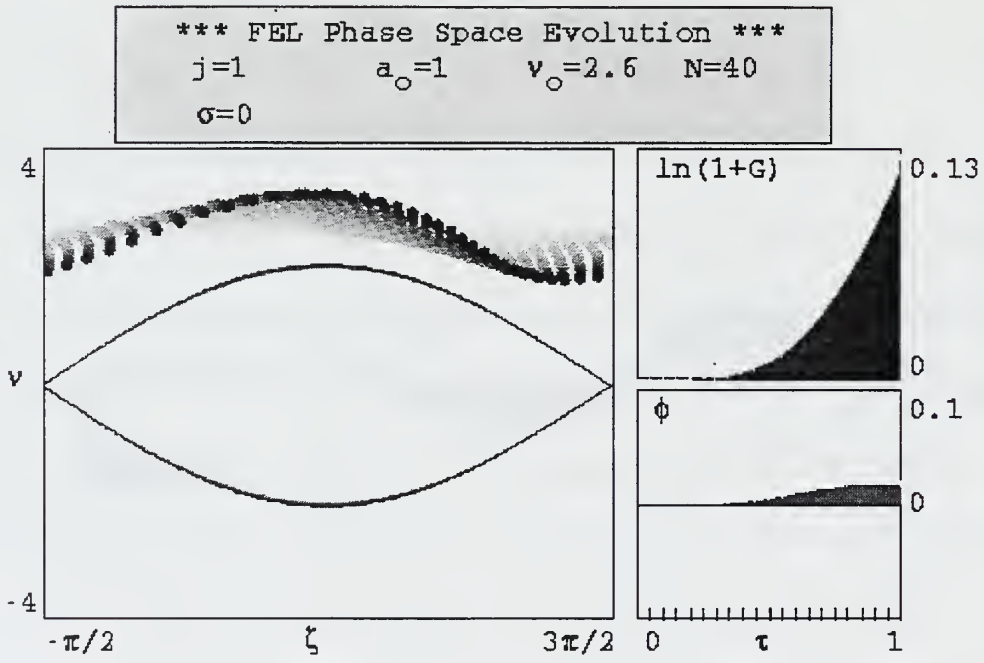

Figure 7. Phase Space Diagram of Maximum Gain for Low Current & Weak Fields

D. GAIN DEGRADATION DUE TO ELECTRON BEAM QUALITY

Until now, a perfect electron beam entering the undulator has been assumed. This means that all electrons enter the undulator with the same initial energy (i.e. the energy spread is $\Delta\gamma/\gamma = 0$) and they enter with zero displacement and angular error from the undulator's z-axis (i.e. the emittance $\varepsilon = 0$).

Concerning FEL performance, (47) states gain increases with increasing current density j. Using (16) and (34), $j \propto IN^3\lambda^{1/2}$, where I is the electron current, so there are three ways to increase j. However, λ is usually fixed for a particular application. In addition, increasing I tends to decrease the beam quality from the accelerator, and increasing N tends to increase the FEL's sensitivity to beam quality by narrowing the gain spectrum bandwidth. So, there exists a trade-off between high current density and good beam quality [7].

To help quantify how poor beam quality affects FEL performance, a Gaussian distribution is assumed for the energy spread using (39) to define the standard deviation as:

$$\sigma_G = \Delta\upsilon = 4\pi N\Delta\gamma/\gamma\,. \tag{49}$$

If two electrons enter the undulator with the same electron phase ζ, they will drift apart by $\Delta\zeta = \Delta\upsilon\Delta\tau$. If $\sigma_G = \Delta\upsilon \approx \pi$, then the phase separation is as much as $\lambda/2$ by the time the two electrons leave the undulator. This impairs bunching significantly reducing gain. The typical energy spreads from a good accelerator is on the order of 10^{-3}.

Gaussians are also assumed to represent displacement and angular errors. Their associated standard deviations are:

$$\sigma_E = \sqrt{\frac{\pi}{\lambda L}}\bar{r}_O \quad \text{and} \quad \sigma_\vartheta = \frac{2\pi N\gamma^2\bar{\vartheta}^2}{1+K^2}, \tag{50}$$

where $\bar{r}_O$ is the electron's rms distance from the z-axis and $\bar{\vartheta}$ is the electron's rms injection angle. As with σ_G, when either of these standard deviations is near π, gain begins to degrade.

E. SHORT PULSE EFFECTS

Most FEL oscillators use short electron pulses rather than a continuous beam. These electron pulses in turn produce a short optical pulse. At the undulator entrance ($\tau = 0$), electron and optical pulses enter together where the electron pulse gives up a portion of its energy. Although both pulses may enter the undulator at the exact same time (i.e. synchronized), their relative positions change as they travel down the undulator. The electron pulse travels somewhat slower than the speed of light so it slips back relative to its starting point with the optical pulse. This slippage distance is approximated by assuming the FEL is at resonance. Resonance, by definition, is when one wavelength of light λ passes over an electron as that same electron travels one undulator wavelength λ_O. By the time the electron exits the undulator, it has slipped back a distance of $N\lambda_O$. If the electron pulse length is comparable to this distance, then the electron-photon interaction is dominated by short pulse effects [8].

If the distance between mirrors is *S*, then an optical pulse arrives at the undulator entrance ($\tau = 0$) in time intervals of *2S/c*. As the optical pulse enters the undulator, the distance ahead of its associated electron pulse is the FEL's desychronism *d*. It is normalized to the slippage distance, and equals:

$$d = -\frac{2\Delta S}{N\lambda_O} \tag{51}$$

Operationally, d is changed by moving one of the mirrors inward by a small amount ΔS. At first thought, d=0 (i.e. synchronized pulses) would seem to result in the most coupling since the peak of the electron pulse would coincide with the optical pulse peak each pass. However, this is not the case. In fact, it results in zero final power! Figure 8 shows the pulse evolution of such a case where the optical power is evolving to zero.

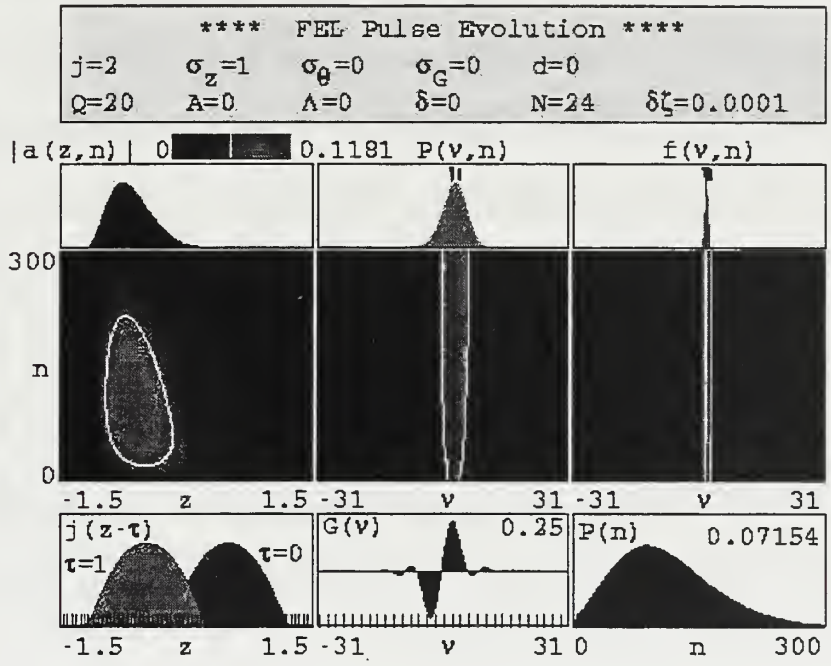

Figure 8. Synchronized Pulse Evolution

To help understand how the electron and optical pulses evolve, the longitudinal coordinate is scaled to the slippage distance by $z / N\lambda \rightarrow z$. This means the optical pulse, travelling at speed c, remains fixed in z while the electron pulse, travelling slower at $\beta_z c$, slips back in z. The lower-left picture of Figure 8 is a graph of the dimensionless

current density j versus z at $\tau = 0$ (dark gray) and at $\tau = 1$ (light gray). The electron pulse is assumed to be parabolic of the form $j(z) = (1 - 2z^2 / \sigma_z^2) j$ for $|z| < \sigma_z / \sqrt{2}$ and zero elsewhere. In Figure 8, $\sigma_z = 1$ and has a maximum value of j=2.

The number of passes through the undulator is represented by n=300 and the cavity power loss per pass is $1/Q = 1/20$. Noise is simulated in Figure 8 by inserting a random phase displacement per electron with rms value of $\delta\zeta = 10^{-4}$. Just above the electron pulse graph is shown the dimensionless optical amplitude a evolution as a function of both z and n. The bottom, middle picture graphs (47) showing gain G as a function of electron phase velocity υ. Just above it is the FEL's power spectrum as a function of n. The middle right graph it is the υ distribution f as a function of n while the graph just below it depicts dimensionless power P as a function of n. The power P is the square of the dimensionless optical pulse amplitude a, and can be converted into a real average power in four steps. First, using the definition of a in (21), the real electric field magnitude E is found. Second, the power density is now known since it equals $E^2 / 8\pi$. Third, the peak power is the power density multiplied by the beam area, and last, the average power is the peak power multiplied by the duty cycle.

The optical pulse initially grows from noise, and is as wide as σ_z plus the slippage distance $\Delta z = 1$. Once the optical pulse form, the electron pulse couples with it, and it intensifies (see the lower right *P(n)* graph in Figure 8). It also narrows (see the middle left plot of $|a(z,n)|$). However, since the electron pulse drifts back, it amplifies the optical pulse's trailing edge on every pass through the undulator. Equation (47)

shows this analytically. Very little gain occurs in the first third of the undulator ($\tau << 1$), and the majority of gain occurs towards the end ($\tau \approx 1$). As stated earlier, gain requires electron bunching, and bunching takes time. The graph of $|a(z,n)|$ shows this as the optical pulse peak decreases in z with each increase in n. Eventually, the optical pulse moves back so far that it decouples from the incoming electron pulses, and dies out around n=300.

To ensure the optical and electron pulses remain coupled, the optical pulse pathlength Δs must be shortened (i.e. $d > 0$). Even a small desynchronism can accomplish the desire effect. Figure 9 uses the same parameters as those in Figure 8 with the desynchronism of d=0.003. Because the optical pulse is advanced for each pass, its position in z remains constant. This allows the electron pulse to "sweep" across the entire optical pulse leaving it undistorted. As a result, the FEL's power grows and eventually levels out to a steady-state value.

Unfortunately, increasing d indefinitely is counter-productive. With increasing d, eventually the optical pulse is advanced so far that it again decouples with the incoming electron pulse reducing steady-state P. For large desynchronism, the optical field has a long exponential tail of the form [8]:

$$|a(z)| \propto e^{-z/4Qd} \tag{52}$$

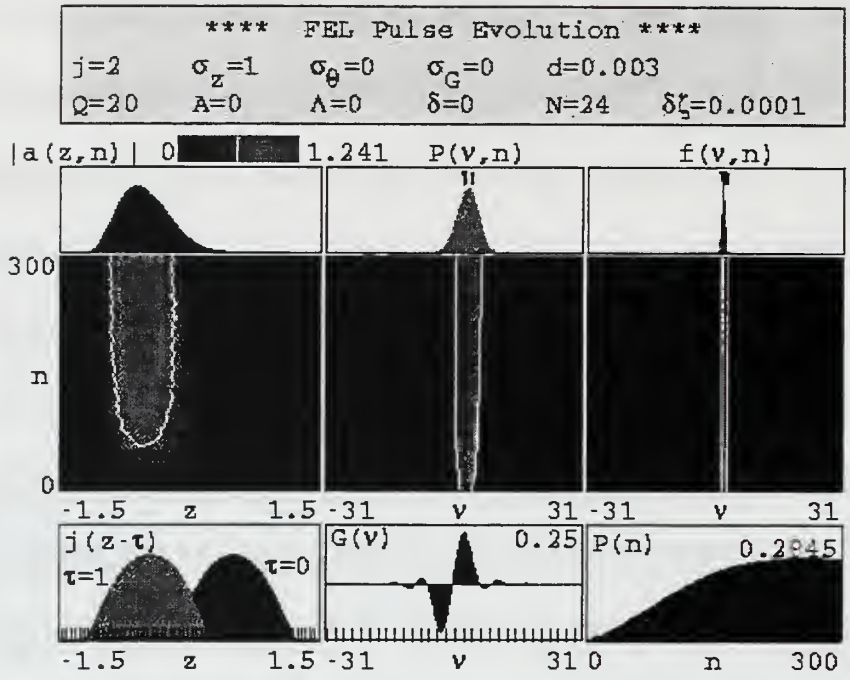

Figure 9. Desynchronized Pulse Evolution

F. THE KLYSTRON UNDULATOR

The klystron is a two-stage undulator specifically designed to improve FEL gain in weak optical fields [9]. Figure 10 shows the design of a klystron undulator. Simply stated, it is nothing more than an conventional undulator cut in half and spread apart to create a drift space between sections. The first section, called the "modulator",

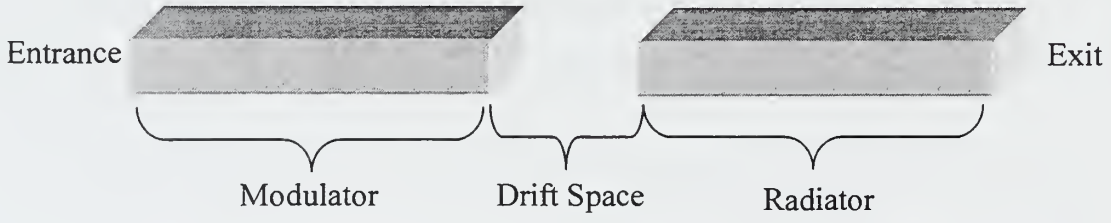

Figure 10. Kylstron Undulator

prepares the electrons for bunching by developing phase velocity differences. The middle section between the conductors provides space for the electrons to bunch as they drift. The final section is called the "radiator" where highly bunched electrons create and amplify the optical field. The drift section can be shortened by using bending magnets (a dispersive section) to reduce overall length [9].

The drift or dispersive section strength is given by the dimensionless parameter:

$$D = \frac{N_d}{N} \tag{53}$$

where N is the number of undulator periods in both the modulator and radiator, and N_d is the drift space length in number of undulator periods. Within the drift space, υ is constant so the only electron phase change is $\Delta\zeta = \upsilon D$. Electron bunching will therefore occur without optical pulse interaction so the optical field remains constant.

Via simulation, the low current gain curve as a function of υ_O can be constructed. Figure 11 shows the gain spectrum with j=1 and D=1. Comparing with Figure 5, the gain increases from 0.13 to 0.37, about three times as much. For jD<1, the gain equation can be approximated near resonance as:

$$G(\upsilon_O) \approx \frac{jD}{4}\sin(\upsilon_O D) \tag{54}$$

The maximum gain therefore becomes $jD/4$ when $\upsilon_O = \pi / 2D$.

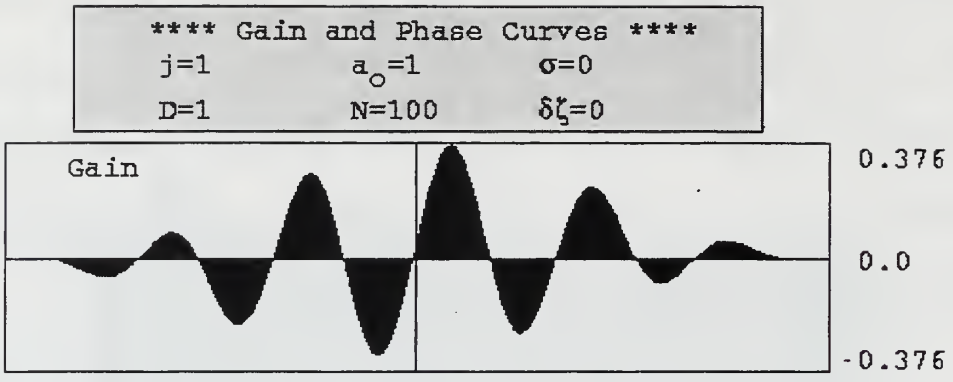

Figure 11. Low Current Klystron Gain Versus Initial Phase Velocity

A negative aspect to using a klystron is that the electron beam quality must be sufficient to keep $\Delta\upsilon_o \leq \pi / D$. Otherwise, the gain is negative. This is a tighter constraint than that placed upon conventional undulators ($\Delta\upsilon_o < \pi$), and can become the limiting design factor when D is large.

III. TJNAF FREE ELECTRON LASER

A. KW FEL DESIGN

As mentioned in the introduction, TJNAF is planning to achieve first light from their kW FEL this summer. Figure 12 is a basic diagram of this laser. Free electrons are

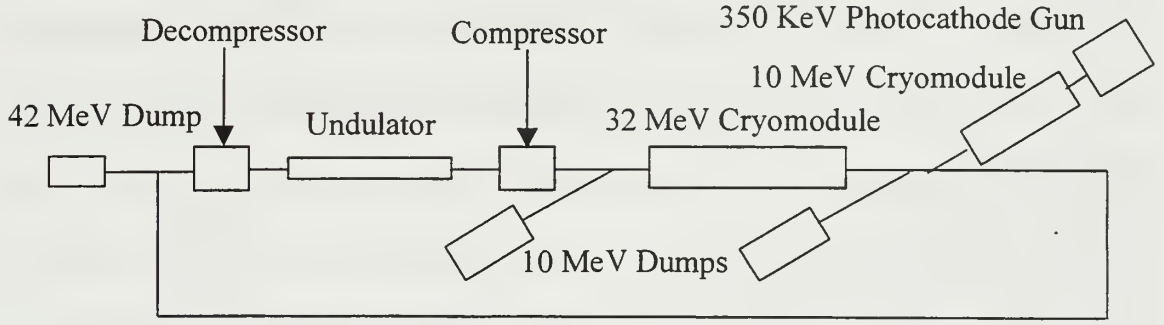

Figure 12. TJNAF kW FEL Design

created from the 350 KeV photocathode gun and initially accelerated in the 10 MeV cryomodule. At this point, they are accelerated further with the 32 MeV cryomodule. As shown in the theory section, shortening the pulse width increases j that in turn improves the gain G. To capitalize on this, electrons are "pre-bunched" using a compressor before entering the undulator. Upon leaving the undulator, electrons are "unbunched" using a decompressor before they enter the first major bend. This helps reduce energy loss whenever electrons change direction. Electrons are eventually sent to one of the three dumps dependant upon the system configuration. The two 10 MeV dumps are used when testing the electron gun and cyromodules. During normal operation, the electrons are sent to the 42 MeV dump following the decompressor. The recirculation ring serves an important purpose by redirecting the electrons back through the 32 MeV cryomodule out of phase. This serves two purposes. First, it conserves energy by using the recirculated

electrons to power in part the cryomodule. This reduces what the cryomodule would otherwise need in RF power. Second, it reduces the beam dump size by removing 32 MeV from the electrons before discarding them.

B. PROPOSED 20 KW FEL PARAMETERS

Following successful demonstration of their kW FEL, TJNAF plans to improve their design to provide 20 kW on target. Table 1 below is a list of proposed parameters to meet this goal, and was used in the simulation work contained herein.

PARAMETER	
Optical Wavelength λ	1.05 μm
Undulator Wavelength λ_O	20 cm
Peak Undulator Magnetic Field B	2 kG
Undulator Periods N	24
Undulator Length L	6 m
Undulator Parameter K	0.79
Dispersive Strength D	1, 2 or 3
Electron Energy γmc^2	200 MeV
Maximum allowed Energy Spread $\Delta\gamma/\gamma$	6 %
Electron Beam Radius r_b	0.5 mm
Electron Pulse Length σ_Z	2.0 ps
Initial Phase Velocity υ_O	0.0 (on resonance)
Initial Electron Phase Velocity Standard Deviation σ_G	0.3
Electron Injection Angle Standard Deviation σ_ϑ	0.15
Peak Current I	200 A
Average Current	8 mA
Current Density j	2
Initial Optical Field a_0	0.0
Cavity losses $1/Q$	0.1
Peak Optical Power within cavity	40 GW
Repetition Rate	74.85 MHz
Duty Cycle	$4x10^{-5}$
Average Optical Power P within cavity	1.6 MW
Required Efficiency for 20 kW on target	1 %

Table 1. TJNAF 20 kW Proposed Parameters

IV. SIMULATION RESULTS

A. KLYSTRON GAIN

The first design goal was to discover the steady-state gain behavior as a function of both dispersive strength D and desynchronism d for a proposed 20 kW klystron. TJNAF provided necessary design parameters as provided in Table 1. TJNAF is considering D's of 1, 2 or 3. LT Richard Steele conducted simulation work for the cases of D=0 (a conventional undulator, no klystron) and 1 [10] while this thesis deals with the cases D=2 and 3. For completeness, the final results of both are combined in the follow-on graph. Desynchronism was examined from d=0.0 (i.e. synchronized pulses) to d=0.3.

The steady state gain behavior was revealed using the pulse evolution output as described in Chapter II, Section E with one exception. Instead of plotting power P as a function of the number of passes n down the undulator, P is replaced with gain G as a function of n. The simulation was run only long enough for gain to reach a steady state value. The results are shown in Figure 13. Desynchronism is plotted along the x-axis with G as the y-axis. Simulations were conducted in steps of d=0.02 for all four dispersive strength cases. The only deviation from Table 1 in design parameters concerned the mirror losses $1/Q$. To shorten the time required for each simulation, mirror losses where neglected by making Q=1x10^{10}. This allowed G to be evaluated accurately.

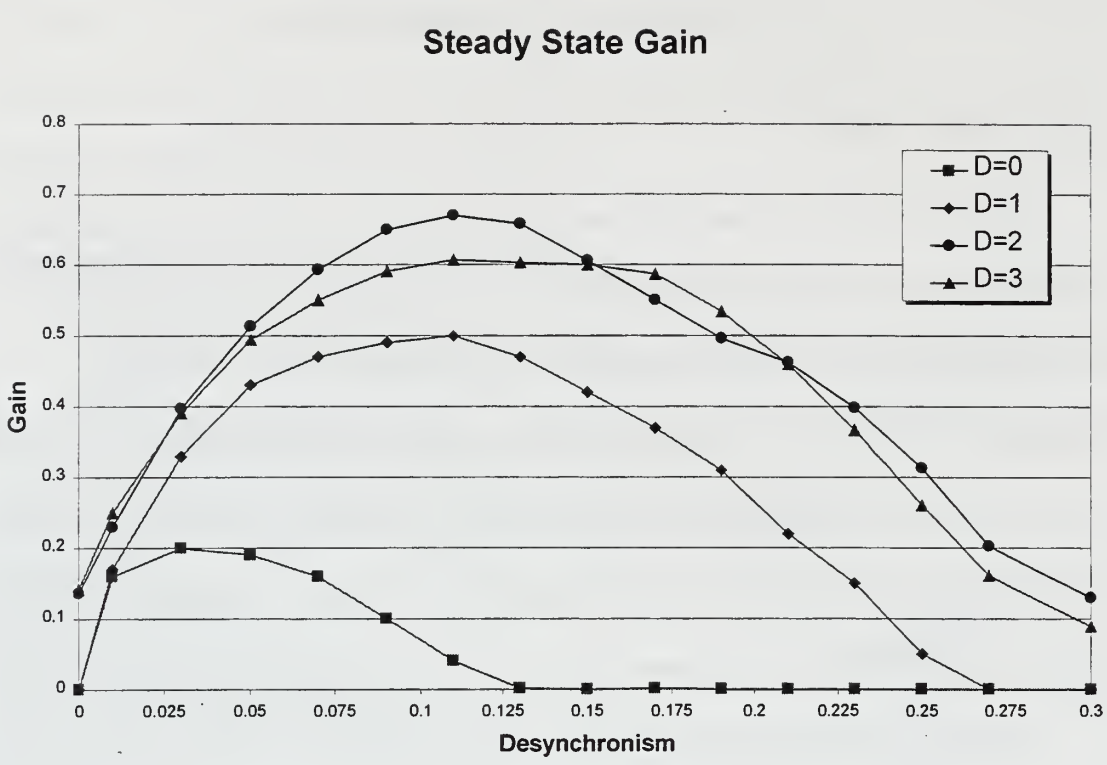

Figure 13. Steady State Gain For Various Dispersive Strengths

For the conventional undulator (D=0) starting at synchronized pulses (d=0), the steady-state gain begins at zero, and then increases to a maximum value of G=0.18 at d=0.03. From there, any further increases in d reduce peak gain until it again is zero at d=0.13.

As shown in Chapter II, Section F, a klystron improves gain in the presence of weak optical fields. Figure 13 quantifies this improvement. With D=1, the klystron provides a 2.5 increase in peak gain (from G=0.18 to G=0.50). One unfortunate consequence is that maximum gain now occurs at a much larger value of d=0.11. Increasing d decreases final power further, as will be seen later. A dispersive strength of D=2 actually provides the most gain: G=0.67. Notice how the maximum gain now occurs at the same d for each D value of 1, 2 or 3.

An interesting phenomenon occurs from D=2 to D=3. Although dispersive strength increases, there is no further increase in steady state gain. Therefore, there appears to be an estimated optimum value of D=2.

B. KLYSTRON POWER AND ENERGY SPREAD

The second design goal is to define the final average optical power as functions of both d and D. Table 1 provided the operating parameters, and the same values as used in gain for D=0, 1, 2 and 3, d in step size of 0.02 between d=0.0 to d=0.3. Again, LT Richard Steele ran simulations for values D=0 and 1 [10], and his final results are included in the following results.

The simulated optical pulse was allowed to evolve to steady state requiring n= 2,000 passes for small d to n=300 passes for large d. The final dimensionless power was read from each output graph, and then converted into a real average power. The results are shown in Figure 14. Desynchronism remains on the x-axis with average power on the y-axis.

From Figure 14, a conventional undulator with D=0 provides the most power. Maximum power occurs at a small value of d=0.01 (see Chapter II, Section E), and the conventional undulator provides 25 times as much as the klystron case for D=1. As mentioned earlier, a klystron improves gain in weak fields, but unfortunately, it is at the expense of final power at saturation.

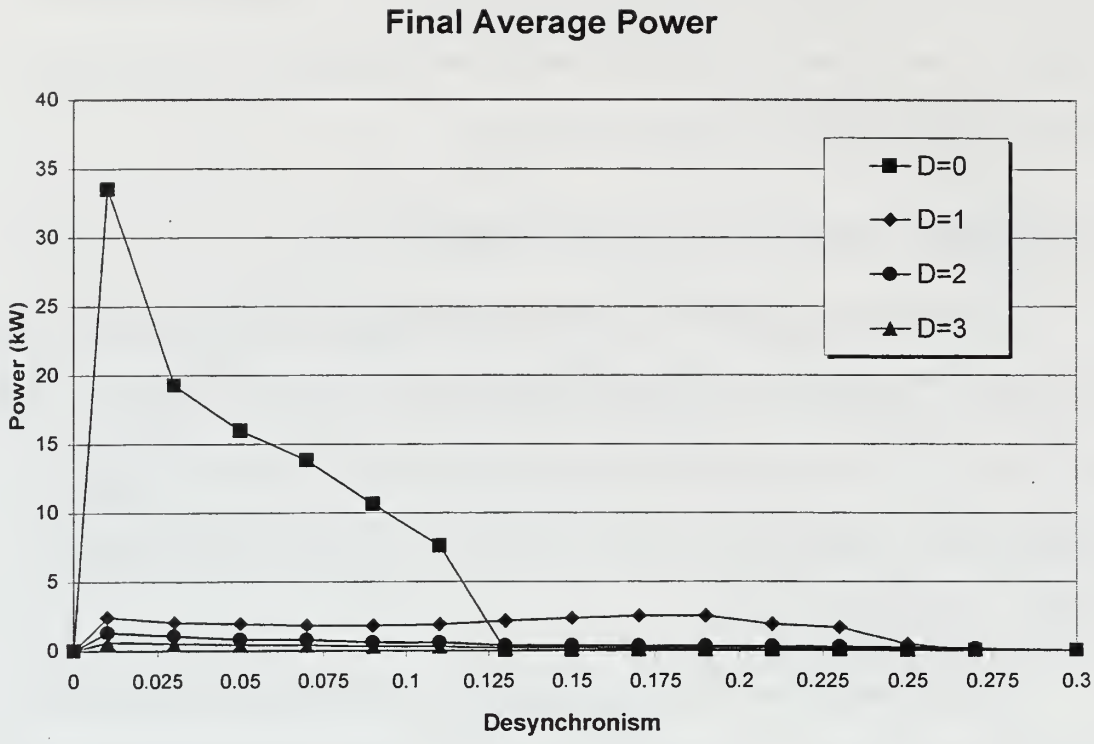

Figure 14. Final Average Power For Various Dispersive Strengths

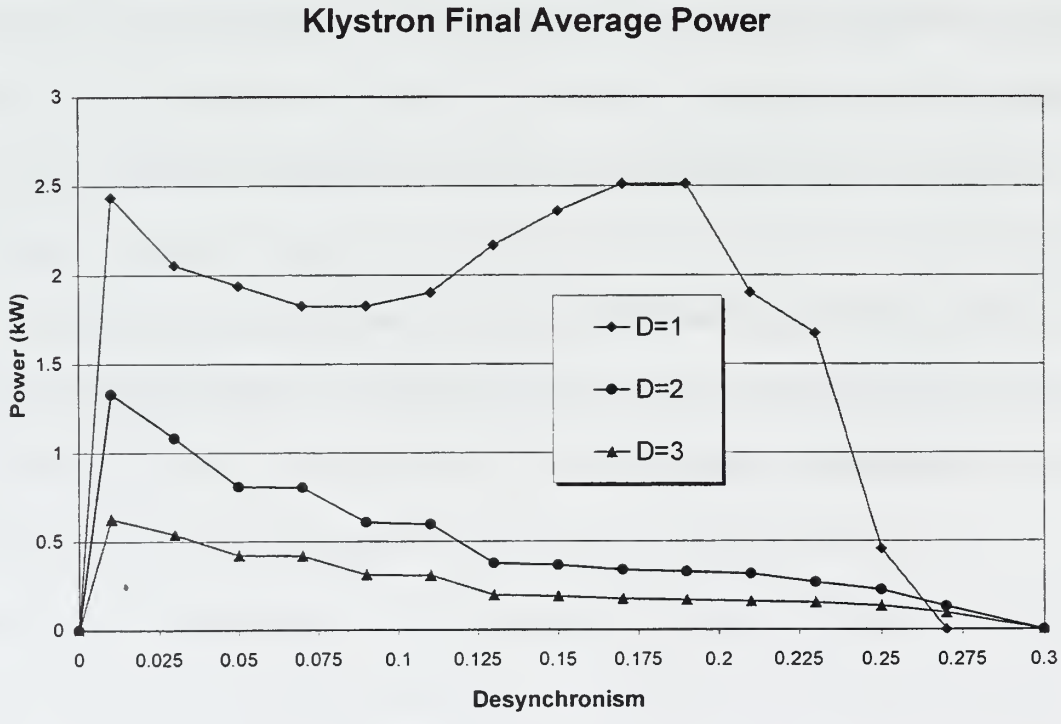

Figure 15. Klystron Final Average Power For Various Dispersive Strengths

Since the conventional undulator provides much more power, why use a klystron at all? Higher powered lasers (kW and above) may use higher cavity to increase output. Therefore, the gain G must be improved to overcome these losses. The first way to increase G is to increase j, but that is limited by the electron gun technology. The klystron provides a secondary means to provide the additional gain required. So while the klystron lowers output power, it may very well be a necessary evil in achieving the required level of gain to make the laser work in the first place.

Since the conventional undulator so dominates the graph, Figure 15 eliminates this case, and allows comparison in terms of power of differing dispersive strengths D. Here, D=1 provides about twice as much power as the case D=2 with diminishing returns shown for D=3. While the cases of D=0, 2 and 3 show an early maximum then tailing off to zero, D=1 exhibits quite irregular behavior. After peaking at d=0.01, it decreases until d=0.13 where then it improves to its highest value at d=0.17. The reason for this is explained at the end of this section.

To understand a little about the power behavior, let us examine a few points on the graph in detail for D=2. First, let us look at d=0.01 where power is maximum. Figure 16 shows the pulse evolution for this point on the graph.

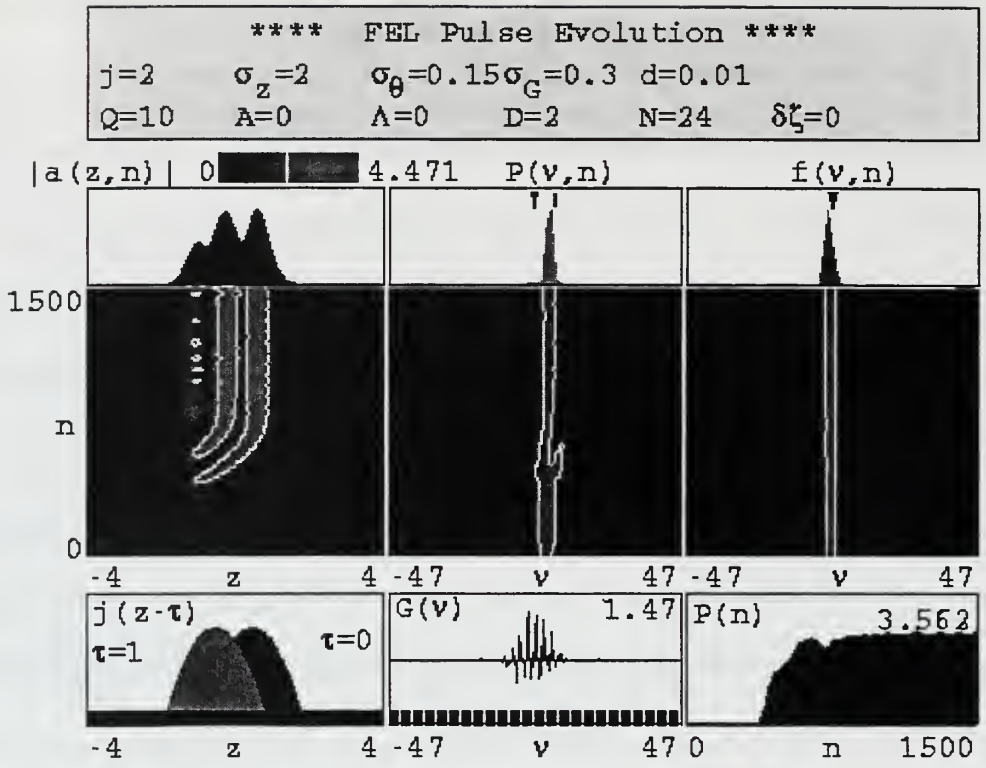

Figure 16. Pulse Evolution For *d*=0.01

For a general explanation of each plot within Figure 16, refer to Chapter II, Section E. Notice how the optical pulse evolves. It begins with one peak, but when n is approximately 650, a second peak forms with equal intensity to the first peak. The power reaches steady-state and the electron υ spread is $\Delta\upsilon = 6.5$.

The third design goal is maintaining energy spread $\Delta\gamma/\gamma$ below 6%. An energy spread of 6% or less is necessary for TJANF to successfully recirculate electrons (see Chapter III for the benefits of recirculation). Using (39), this translates into an energy spread of $\Delta\gamma/\gamma = 2\%$ that is well within the design requirement of 6%. Surprisingly for D=2 and D=3, the energy spread is constant at 2% for all values of desynchronism. On the other end of the desynchronism scale, Figure 17 shows the pulse evolution for d=0.13.

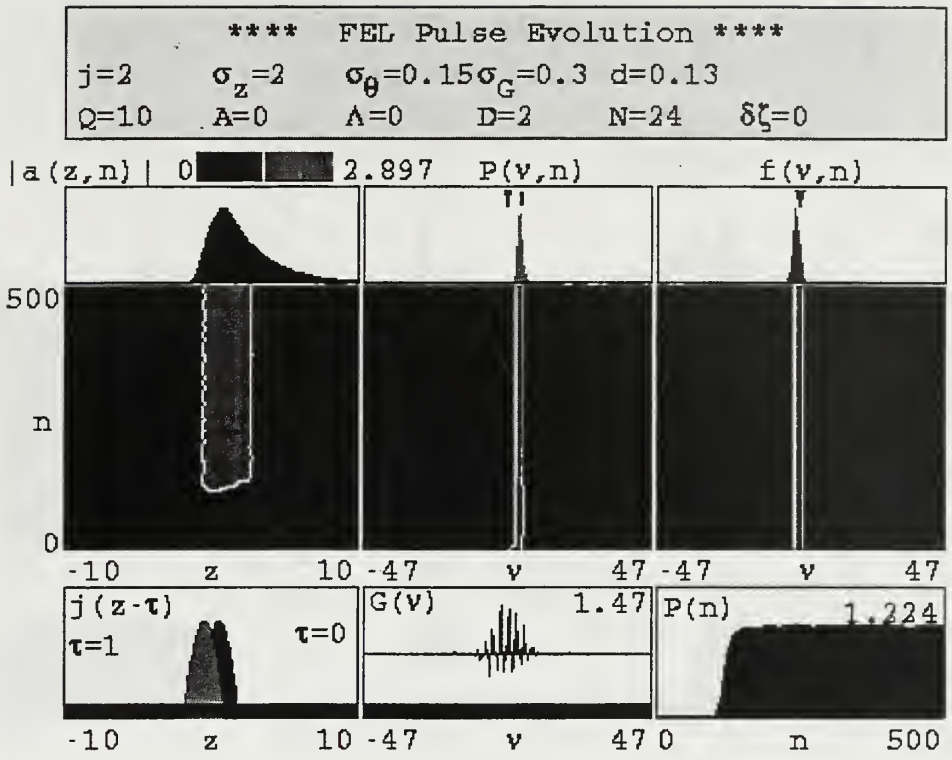

Figure 17. Pulse Evolution For *d*=0.13

Here, there is only one peak with a long exponential ramp formed ahead of the main pulse. While the power P reaches steady-state quite early at $n \approx 100$ passes, it is only a third of its maximum value in Figure 16 at d=0.01. The optical pulse retains this kind of shape with further increases in d, but declines gradually to zero amplitude at d=0.3.

In between the d values of 0.01 and 0.13, the optical pulse exhibits erratic performance. Figure 18 shows such an intermediate case with d=0.07. The transformation is taking place from a two peak optical pulse to a one peak pulse. This is also an example of trapped particle instability [11].

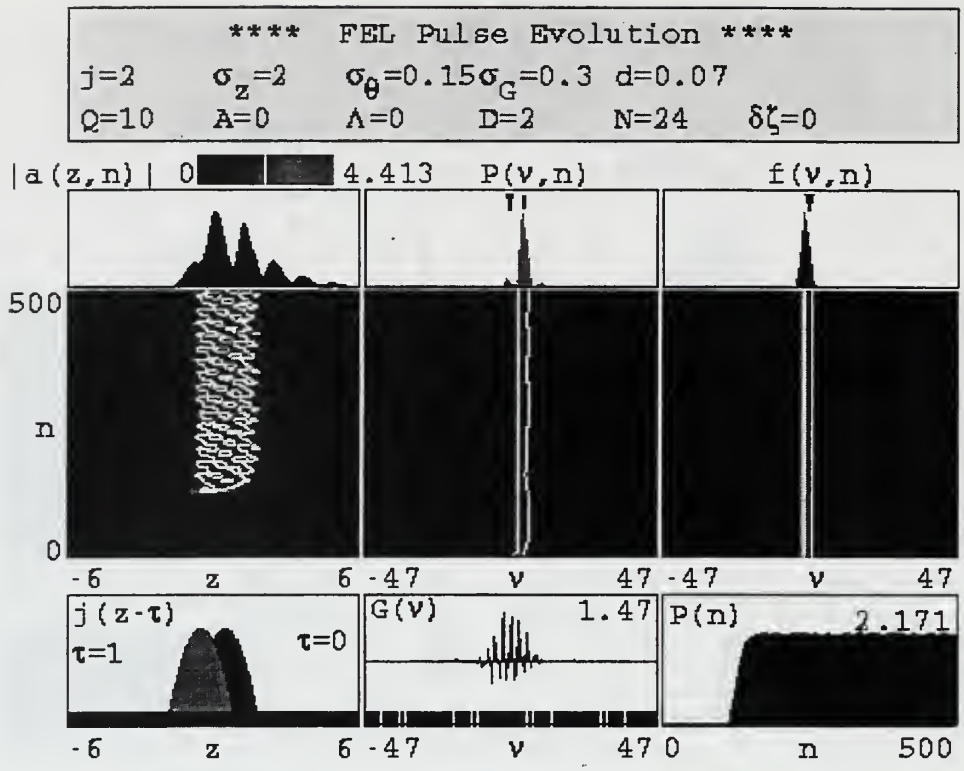

Figure 18. Pulse Evolution for *d*=0.07

The trapped-particle instability occurs when electrons, in the presence of strong optical fields ($a \geq \pi$), become trapped within potential wells in phase space. These electrons begin to oscillate at the "synchrotron" frequency $\upsilon_S \approx |a|^{1/2}$ [11]. This behavior causes the beam current to oscillate that in turn drives modes at sideband frequencies of $\upsilon_O \pm \upsilon_S$, shifted away from the fundamental wavelength by $\Delta\lambda / \lambda = \upsilon_S / 2\pi N$. These sidebands can be seen in Figure 18's power spectrum $P(\upsilon, n)$.

Now recall the power curve for the case *D*=1 in Figure 15. It reaches a peak at *d*=0.01, declines, and then increases again from *d*=0.1 to 0.2 before finally diminishing to zero at *d*=0.27. From [10], examining the optical pulse shape with increasing *d* yields an explanation for this behavior. Although the optical pulse amplitude peak decreases in the

region d=0.1 to 0.2, the exponential ramp of the form shown in (52) is extending at a greater rate as d increases. This leads to an overall increase in final average power. However, increasing d beyond 0.2 provides a rapid decrease in peak amplitude too great for the extended pulse shape to overcome. A rapid decrease in average power results until at large d there is no laser power.

V. CONCLUSIONS

The purpose of this study was to quantify the behaviors of steady-state gain, final average power and energy spread as functions of desynchronism d and dispersive strength D for a proposed 20 kW klystron free electron laser (FEL). This proposal is under consideration by the Thomas Jefferson National Accelerator Facility (TJNAF) to improve the kW FEL they are now constructing. Design parameters are listed in Table 1. These conclusions combine the work contained herein with reference [10].

The two major design goals were an average optical power of 20 kW while maintaining a final energy spread of 6% or less. The conventional undulator with a desynchronism d=0.03 will achieve these goals.

Gain peaks in desynchronism at d=0.05 for D=0 and at d=0.11 for D=1, 2 and 3. Gain is proportional to dispersive strength up to an estimated optimal value of D=2. Further increases in D result in diminishing gain. A klystron with D=2 provides 30% more gain than D=1 and 70% more than a conventional undulator.

The conventional undulator provides 25 times as much power as a klystron with D=1. Overall, power is inversely proportional to D with D=1 providing twice as much as D=2 and almost 4 times as much as D=3. For D=1, peak power occurs at d=0.17, and falls off rapidly to zero at d=0.25. For D=2 or 3, the undulator's power peaks early at d=0.01, and then gradually declines to zero at d=0.3.

Energy spread is 2% for D=2 or 3 for all values of desynchronism. The energy spread exceeds the design goal of 6% only for the case D=0 within the range d=0.01 to d=0.03.

LIST OF REFERENCES

[1] Colson, W. B., Physics 4911 Course Notes, Naval Postgraduate School, Summer Quarter, 1997.

[2] Colson, W. B. in *Laser Handbook*, Vol. 6, Chapter 5, editors W. B. Colson, C. Pellegrini and A. Renieri, North-Holland, 1990, pp. 132-134.

[3] Colson, W. B. in *Laser Handbook*, Vol. 6, Chapter 5, editors W. B. Colson, C. Pellegrini and A. Renieri, North-Holland, 1990, pp. 129-132.

[4] Jackson, J., *Classical Electrodynamics*, John Wiley and Sons, Inc., New York, 1975, pp 222.

[5] Colson, W. B. in *Laser Handbook*, Vol. 6, Chapter 5, editors W. B. Colson, C. Pellegrini and A. Renieri, North-Holland, 1990, pp. 134-140.

[6] Colson, W. B. in *Laser Handbook*, Vol. 6, Chapter 5, editors W. B. Colson, C. Pellegrini and A. Renieri, North-Holland, 1990, pp. 140-144.

[7] Colson, W. B. in *Laser Handbook*, Vol. 6, Chapter 5, editors W. B. Colson, C. Pellegrini and A. Renieri, North-Holland, 1990, pp. 145-149.

[8] Colson, W. B. in *Laser Handbook*, Vol. 6, Chapter 5, editors W. B. Colson, C. Pellegrini and A. Renieri, North-Holland, 1990, pp. 176-180.

[9] Colson, W. B. in *Laser Handbook*, Vol. 6, Chapter 5, editors W. B. Colson, C. Pellegrini and A. Renieri, North-Holland, 1990, pp. 160-162.

[10] Steele, R. B., Master's Thesis, Naval Postgraduate School, 1998.

[11] Colson, W. B. in *Laser Handbook*, Vol. 6, Chapter 5, editors W. B. Colson, C. Pellegrini and A. Renieri, North-Holland, 1990, pp. 168-175.

INITIAL DISTRIBUTION LIST

1.	Defense Technical Information Center 8725 John J. Kingman Rd., STE 0944 Ft. Belvoir, VA 22060-6218	2
2.	Dudley Knox Library Naval Postgraduate School 411 Dyer Rd Monterey, CA 93943-5101	2
3.	Professor William B. Colson, Code PH/Cw Department of Physics Naval Postgraduate School Monterey, CA 93943-5000	4
4.	Professor Robert L. Armstead, Code PH/Ar Department of Physics Naval Postgraduate School Monterey, CA 93943-5000	1
5.	John Albertine 109 Kingswood Rd Annapolis, MD 21401	1
6.	Joung R. Cook Research Physicist, Code 6655 Naval Research Laboratory 4555 Overlook Dr, SE Washington, DC 20375-5000	1
7.	Fred Dylla TJNAF 12000 Jefferson Ave Newport News, VA 23606	1
8.	George Neil TJNAF 12000 Jefferson Ave Newport News, VA 23606	1
9.	R. Eric LeGear 2909 Snively Rd Yellow Springs, OH 45387	2